CLASSIFICATION AND INSPECTION OF MILLING SURFACE ROUGHNESS BASED ON A BROAD LEARNING SYSTEM

Runji Fang, Huaian Yi, Shuai Wang, Yilun Niu

School of Mechanical and Control Engineering, Guilin University of Technology, Guilin, 541006, People's Republic of China (18894719154@126.com, ✉ yihuaian@126.com, +182 7838 6857, 604994407@qq.com, 3493364331@qq.com)

Abstract

Current vision-based roughness measurement methods are classified into two main types: index design and deep learning. Among them, the computation procedure for constructing a roughness correlation index based on image data is relatively difficult, and the imaging environment criteria are stringent and not universally applicable. The roughness measurement method based on deep learning takes a long time to train the model, which is not conducive to achieving rapid online roughness measurement. To tackle with the problems mentioned above, a visual measurement method for surface roughness of milling workpieces based on broad learning system was proposed in this paper. The process began by capturing photos of the milling workpiece using a CCD camera in a normal lighting setting. Then, the train set was augmented with additional data to lower the quantity of data required by the model. Finally, the broad learning system was utilized to achieve the classification prediction of roughness. The experimental results showed that the roughness measurement method in this paper not only had a training speed incomparable to deep learning models, but also could automatically extract features and exhibited high recognition accuracy.

Keywords: broad learning system, classification, milling surface roughness, rapid training.

1. Introduction

Any machined surface has the unevenness of tiny peaks and valleys, and the unevenness is generally expressed in terms of surface roughness parameters. The size of the surface roughness has a great influence on the corrosion resistance, fatigue resistance and service life of the part [1, 2]. Therefore, it is important to measure the surface roughness of parts accurately and quickly. The most frequently used roughness measuring techniques are classified as contact and non-contact measurements [3]. However, the contact measurement method has the disadvantage of the small detection range, low measurement efficiency and potential for scratching the workpiece. In contrast, non-contact measurement, which has the advantages of high flexibility, fast measurement speed, and support for in-line measurement, is increasingly being relied upon in

precision manufacturing. Non-contact measurement methods mainly include optical measurement, electronic measurement and machine vision measurement. However, optical and electronic measurements have the shortcomings of expensive equipment, low efficiency, and vulnerability to environmental influences [4, 5]. Machine vision measurement is a method based on the optical imaging principle. Its measurement process is not only easy to automate and efficient but also supports online measurement. Therefore, it is significant to study efficient and low-cost machine vision roughness measurement methods. For extracting features using image gray value information, Liu *et al.* [6] constructed a GLCM-SVM model for measuring the surface roughness of deep holes using the GLCM family of indices as the input to a support vector machine. Tsai *et al.* [7] proposed five spectrum indices to characterize roughness and input them into a neural network to predict milling surface roughness. In terms of extracting features using image color information, Yi *et al.* [8, 9] proposed an algorithm for evaluating the sharpness of color images and an average color difference algorithm, and constructed a relationship model between such indices and roughness. To evaluate the roughness of grinding surfaces, Zhao *et al.* [10] proposed a detection method based on the singular value entropy of color images. Although the above-mentioned index-based roughness prediction methods are effective, there are common limitations such as difficulty in index design, significant human influence factors, and demanding image acquisition environment. Because of these drawbacks, such measurement methods cannot be directly applied to complex and changing industrial applications. As a result, the visual roughness measuring approach with high measurement accuracy and the ability to extract features automatically has become a hot research topic.

In recent years, deep convolutional neural networks have become increasingly capable of expressing image features. Deep learning models are gradually being introduced into the field of roughness measurement due to their ability to automatically extract image features. Chen *et al.* [11] used a deep convolutional neural network to achieve index-free roughness detection. Rifai *et al.* [12] proposed a method to evaluate surface roughness directly from surface texture images using convolutional neural networks. Yan *et al.* [13] proposed a roughness measurement method based on image segmentation for helical gear surfaces, and the extracted effective image regions were fed into a convolutional neural network to evaluate their roughness. Although the above-mentioned roughness measurement methods based on deep convolutional neural networks realized automatic feature extraction and guaranteed good accuracy, they also have shortcomings. Due to a large number of connection parameters in the filters and layers of deep convolutional neural networks, their training process is extremely time-consuming and not suitable for fast-judging roughness online measurement. The *random vector functional-link neural network* (RVFLNN) proposed by Pao *et al.* [14] effectively eliminated the drawback of the long training time, and has been used to solve problems in different domains. However, the RVFLNN cannot handle large-scale data well, so it is not suitable for direct use in the field of visual roughness measurement. The *broad learning system* (BLS) combines the advantages of a deep convolutional neural network and the RVFLNN, which can solve the above problems effectively. The BLS uses the RVFLNN design concept to replace the deep network structure with a flat network shape, which minimizes the number of parameters that need to be optimized and significantly reduces the time it takes to train the model.

Aiming at overcoming the drawbacks of index design-based and deep learning network-based roughness measurement methods such as difficult index design, considerable human influence factors and slow model training speed, a visual measurement method for surface roughness of milling workpiece based on the BLS was proposed in this paper. Milling workpiece images built in the BLS were captured by an industrial camera under normal light sources and combined with data enhancement techniques to reduce the model's data volume requirements. Then a broad

learning network was used to automatically extract features and rapidly train the model. Finally, a surface roughness measurement model applicable to milling workpieces was obtained, and a fast end-to-end measurement was realized.

2. Theoretical basis of predictive modeling

2.1. Analysis of milling surface morphology

Due to the consistency of the tool edge in milling processing, the arrangement of the tiny peaks and valleys on the processing surface is regular, which is mainly caused by the regular vibration of the machine tool [15]. Likewise, the feed motion of the tool creates a clear texture on the surface of the workpiece. In this paper, the milling specimens with *Ra* 0.236 μm and *Ra* 1.477 μm were magnified 500 times by using a VHX1000 ultra-deep field 3D microscope to obtain the surface texture maps of the two specimens, respectively. Then a JB-4C stylus roughness tester was used to make a single measurement on the milling workpiece surface to get the up and down fluctuation map of the stylus. Finally, the Zygo NewView™7100 white light interferometer was used to scan the machined surface to get a 3D morphology map. Various graphs of the two milling specimens are shown in Fig. 1.
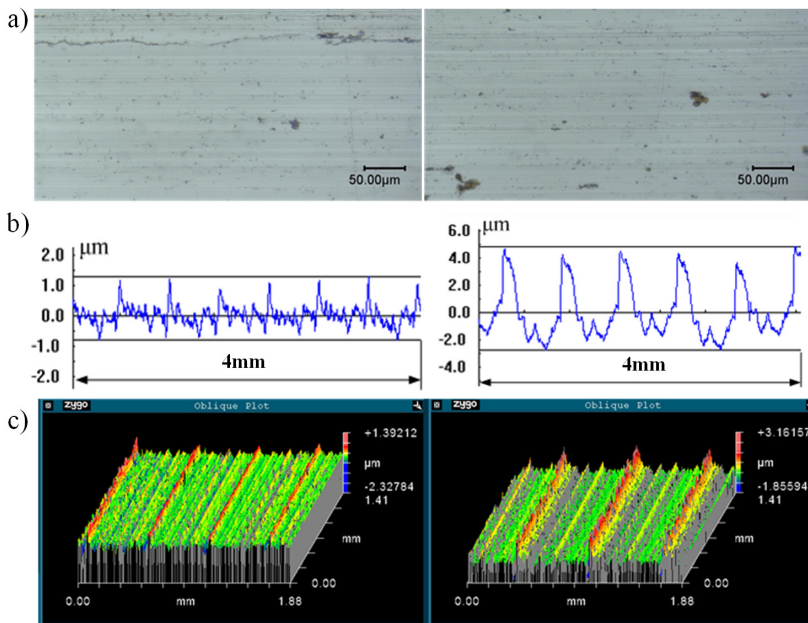
Fig. 1. Milling specimen (Left *Ra* 0.236 μm, Right *Ra* 1.477 μm). a) Microscopic surface topography, b) roughness stylus measurement fluctuation graph, c) surface 3D morphology.

From Fig. 1a, it can be seen that the difference between the microscopic morphology of the milling surface with different roughness was not significant under human eye observation when the milling surface roughness was *Ra* 0.236 μm and *Ra* 1.477 μm, respectively. During the linear measurement of roughness with the stylus (Fig. 1b), however, there was a distinct disparity between the peak value and the fluctuation frequency, despite the stylus fluctuating up and down

fairly consistently. Two cases are considered here. (1) When the roughness was small, the peak was smaller and the crest was larger. (2) When the roughness was larger, the peak was larger and the crest was smaller.

Their surface 3D morphology is shown in Fig. 1c, the joint marks representing the profile peak height are indicated by red lines, and the cutting surface representing the profile flatness is indicated by yellow-green lines. The difference between the two was very large, as shown in Fig. 1c, despite the fact that the height distribution of the milling surface profile was very regular. Again, two cases are under consideration. (1) When the roughness was equal to Ra 0.236 μm, the height distribution was relatively uniform and the surface was relatively flat. (2) When the roughness was equal to Ra 1.477 μm, the joint tool marks were spaced like a high wall separating the cutting surface and the flatness was poor. Generally speaking, the milling surface topography also showed a certain regular change with the change of roughness.

The theoretical basis of machine vision inspection is the principle of light reflection on the surface of a workpiece. The incident light from the light source is reflected by the workpiece surface and then received by the vision sensor to form an image of the workpiece surface. The image quality is determined by the light reflection properties of the workpiece surface which, in turn, depend on the microscopic surface topography. Microscopic morphology is generally characterized by surface roughness parameters. Therefore, the correlation between milling surface topography and roughness provides a theoretical basis for machine vision applied to milling workpiece roughness measurement.

2.2. Broad learning system principle

To improve the model training speed, Chen *et al.* [16] proposed the BLS based on the RVFLNN whose basic structure is shown in Fig. 2.
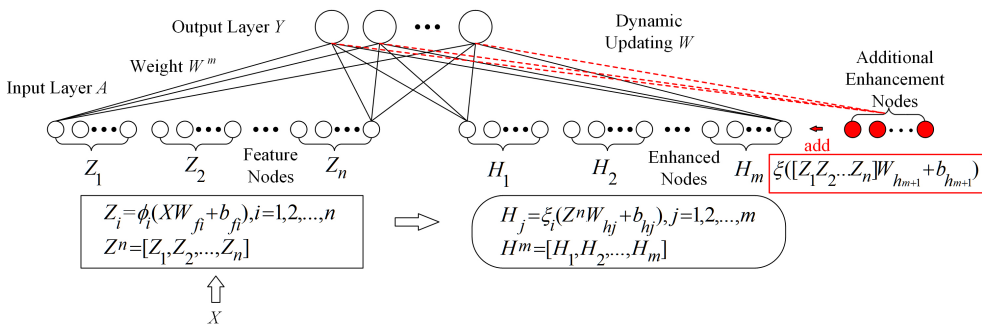
Fig. 2. Basic structure of broad learning system.

In Fig. 2, X is the input data, Z_i is the feature node, H_j is the enhancement node, and W is the connection weight between the input layer A and the output layer Y. The specific design ideas are as follows. Firstly, the input data X is feature-mapped to obtain random features Z_i, $i = 1, 2, \ldots, n$, where n is the number of mapped features, as shown in (1).

$$\begin{cases} Z_i = \phi_i \left(X W_{f i} + b_{f i} \right), & i = 1, 2, \ldots, n \\ Z^n = [Z_1, Z_2, \ldots, Z_n] \end{cases}, \tag{1}$$

where ϕ_i is the mapping function, $W_{f i}$ is the random weight matrix, $b_{f i}$ is the random bias matrix, and Z^n is the set of feature nodes obtained by merging n groups of feature nodes $Z_1, Z_2, \ldots, Z_n$.

Then Z^n is enhanced with features to obtain the enhanced node H_j, as shown in (2).

$$\begin{cases} H_j = \xi_i \left(Z^n W_{hj} + b_{hj} \right), & j = 1, 2, \ldots, m \\ H^m = [H_1, H_2, \ldots, H_m] \end{cases}, \tag{2}$$

where ξ_i is the enhancement function, W_{hj} is the random weight matrix, b_{hj} is the random bias matrix, and H^m is the set of enhancement nodes obtained by merging m sets of enhancement nodes $H_1, H_2, \ldots, H_m$. Finally, the algorithm of the BLS is represented as follows.

$$Y = \left[Z_1, Z_2, \ldots, Z_n | H_1, H_2, \ldots, H_m \right] W = [Z^n | H^m] \, W, \tag{3}$$

where $[Z^n|H^m]$ are the total nodes, W is the connection weight matrix between the input layer A and the output layer Y. Taking $A = [Z^n|H^m]$, (3) can be represented as $Y = AW$. The BLS can be reduced to the following minimization problem based on the generalized inverse calculation of the ridge regression approximation [17].

$$\min_W \|Y - AW\|_2^2 + \lambda \|W\|_2^2, \tag{4}$$

where λ is the regularization factor which prevents overfitting of the function and thus enhances the generalization ability. If the fitting ability of the initial developed model is insufficient, the nonlinear fitting ability is boosted by adding feature nodes or enhancement nodes. Since the update of the weight matrix W_{n+1} uses W_n before the update, it effectively reduces the computational effort of updating the weights and the update is faster. The advantage of broad learning is significant compared to the iterative training of deep learning.

2.3. Data enhancement of milling workpiece surface images

In general, a train set is used to estimate the parameters in the model, which is able to reflect the reality and thus predict the future or other unknown information. And the test set is used to evaluate the predictive performance of the model. Similar to deep neural networks, the BLS also requires a large amount of training data to obtain the desired results. When less milling data is available, the data augmentation algorithm can be utilized to augment the train data set. A data augmentation algorithm can increase the number and diversity of samples, reduce the strong dependence of the model on certain specific attributes to improve the robustness of the model, and enhance the generalization ability of the model. The analysis of the milling surface morphology and the milling workpiece image (Fig. 3) showed that the surface texture characteristics of the milling workpiece mainly exhibited periodic repetition and texture direction consistency. According to the texture characteristics of the milling surface, the image data enhancement methods used were mainly classified into contrast adjustment, hue adjustment, saturation adjustment, brightness adjustment, and rotation adjustment, *etc*. It should be noted that the milling workpiece images of the test set do not use data enhancement in order to be consistent with the actual inspection environment. Some of the effects are shown in Fig. 3.

1. Contrast is the ratio of black to white of the image. When the ratio is larger, the richer is the color expression (5).

$$\text{Contrast} = \sum_\delta \delta(i, j)^2 P_\delta(i, j), \tag{5}$$

where $\delta(i, j) = |i - j|$ is the gray level difference between adjacent pixels, and $P_\delta(i, j)$ is the probability of pixel distribution where the gray level difference between adjacent pixels is δ.

R. Fang et al.: CLASSIFICATION AND INSPECTION OF MILLING SURFACE ROUGHNESS BASED ON A BROAD LEARNING . . .

2. Hue is determined by which wavelength dominates in the light reflected from an object. Different wavelengths produce different color vision, which determines the fundamental characteristics of color nature. r, g, and b are red pixel value, green pixel value, and blue pixel value, respectively (6) and (7).

$$\max = \max(r, g, b), \qquad \min = \min(r, g, b) \tag{6}$$

$$\text{Hue} = \begin{cases} 0°, & \text{if } \max = \min \\ 60° \times \dfrac{g - b}{\max - \min} + 0°, & \text{if } \max = r \text{ and } g \geq b \\ 60° \times \dfrac{g - b}{\max - \min} + 360°, & \text{if } \max = r \text{ and } g < b \\ 60° \times \dfrac{b - r}{\max - \min} + 120°, & \text{if } \max = g \\ 60° \times \dfrac{r - g}{\max - \min} + 240°, & \text{if } \max = b \end{cases} \tag{7}$$

3. Saturation refers to the degree of vividness of the color, also known as the purity of the color (8).

$$\text{Saturation} = \begin{cases} 0°, & \text{if } \max = 0 \\ \dfrac{\max - \min}{\max} = 1 - \dfrac{\min}{\max}, & \text{otherwise} \end{cases} \tag{8}$$

4. Brightness refers to the light and darkness of the light shining on the scene or image (9).

$$\text{Brightness} = 0.299 \times r + 0.587 \times g + 0.114 \times b. \tag{9}$$

5. Rotation. Assume that any point $A_o(x_o, y_o)$ of the original image is rotated by an angle to a new position $A(x, y)$ (10).

$$\begin{cases} x = x_o \cos \beta + y_o \sin \beta \\ y = -x_o \sin \beta + y_o \cos \beta \end{cases}. \tag{10}$$
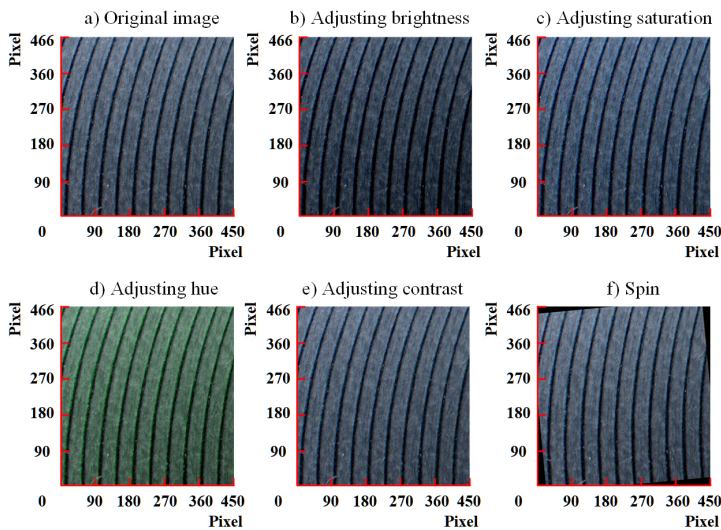
Fig. 3. Partial data enhancement effect diagram.

2.4. BLS roughness measurement model

The BLS roughness measurement model integrates feature extraction, feature transformation and feature classification, omitting the step of the human-designed index. It also greatly reduces the time to train the model and realizes the fast measurement of surface roughness of the end-to-end milling workpiece.

Fig. 4 shows the algorithm flow of the BLS roughness measurement model. (1) The milling workpiece image data set was divided into train set and test set for training and testing of the model, respectively. (2) The number and diversity of training samples were increased by the data enhancement algorithm. (3) The training data and the testing data were normalized. (4) The normalized training data and testing data were fed into the BLS network for learning and the detailed procedure was as follows. The input milling sample X is feature-mapped to create the mapped feature group, which is then coupled to the nonlinear activation function to create the feature augmentation group. The mapped feature group and the augmented feature group are connected to the weight matrix, and then act together on the output layer to get the output Y of the BLS model. (5) The original data was compared with the predicted data to determine the prediction accuracy of the BLS for milling data. (6) The testing time was utilized to demonstrate the superiority of the BLS model's training speed, and the results were compared to those of other prediction models.
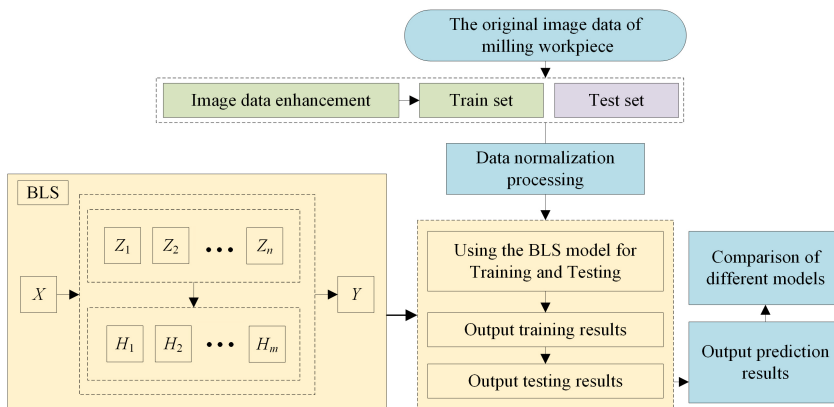
Fig. 4. Algorithm flow chart of the BLS roughness measurement model.

3. Experiment

The experimental procedure of this paper, as shown in Fig. 5, is divided into five parts i.e., preparation of experimental specimens, Roughness measurement, Acquisition of milling workpiece images and making of data set, Comparison experiments, Analysis and discussion of experimental results.
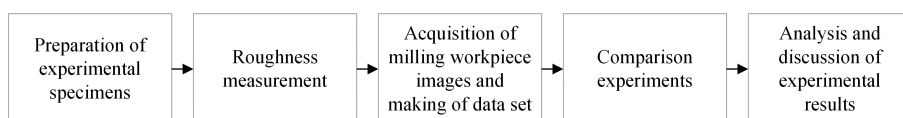
Fig. 5. Experimental flow chart.

www.czasopisma.pan.pl   PAN   www.journals.pan.pl
POLSKA AKADEMIA NAUK

R. Fang et al.: CLASSIFICATION AND INSPECTION OF MILLING SURFACE ROUGHNESS BASED ON A BROAD LEARNING. . .

3.1. Preparation of experimental specimens

The milling specimens for this experiment were machined by an XHS7145 CNC machine tool (Fig. 6a), and a TAP400R100-32-6T milling tool was used (Fig. 6b), with a milling depth of 0.1 mm, feed rate of 200–1100 mm/min, rotational speed of 600 r/min, material 45# steel, size of 60 mm × 40 mm, and the number of specimens produced 30 (Table 1).
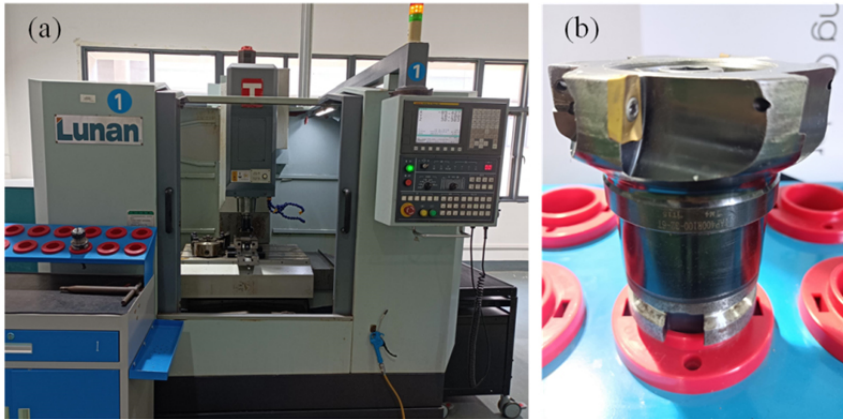
Fig. 6. (a) XHS7145 CNC machine. (b) TAP400R100-32-6T Disc Milling Cutter.

Table 1. Material and processing parameters.

Material	Size	Amount produced	CNC machine type
45# steel	60 mm × 40 mm	30	XHS7145
Milling cutter type	Milling depth	Feed rate	Rotational speed
TAP400R100-32-6T	0.1 mm	200–1100 mm/min	600 r/min

3.2. Roughness measurement

The surface roughness of 30 milling workpieces was obtained by using a stylus roughness measuring instrument TR210 for six times uniformly distributed measurements, and the roughness assessment parameter was Ra. The average value of the six measurements was taken as the surface roughness of the workpiece, and the measurement results are shown in Table 2.

Due to the inherent features of stylus roughness measurement and milling surface topography, the roughness measured with a stylus at various points changes within a specific range. Therefore, in the International Standards Organization (ISO, 1302) standard, the roughness classes commonly used in industrial production are 0.4, 0.8, 1.6, 3.2, 6.3 µm, *etc*., which means that the roughness classes are classified as [0, 0.4], [0.4, 0.8], [0.8, 1.6], [1.6, 3.2], [3.2, 6.3]. In this paper, the roughness was divided into five roughness classes according to intervals [1.0, 1.4], [1.4, 1.9], [1.9, 2.5], [2.5, 3.1] and [3.1, 3.7], which were recorded as R1, R2, R3, R4 and R5, respectively, following the ISO standard and combined with the actual roughness value range in Table 2.

Table 2. Surface roughness of milling workpiece (*Ra*, Unit: μm)

NO	First	Second	Third	Forth	Fifth	Sixth	Average
1	1.310	1.289	1.295	1.290	1.260	1.313	1.293
2	1.063	1.130	1.120	1.122	1.095	1.107	1.106
3	1.077	1.065	1.108	1.028	1.105	1.084	1.078
4	1.378	1.381	1.304	1.306	1.351	1.332	1.342
5	1.214	1.222	1.284	1.213	1.297	1.262	1.249
6	1.221	1.200	1.164	1.154	1.195	1.159	1.182
7	1.483	1.466	1.484	1.447	1.496	1.493	1.478
8	1.440	1.599	1.529	1.483	1.435	1.561	1.508
9	1.595	1.524	1.527	1.558	1.563	1.605	1.562
10	1.433	1.404	1.363	1.471	1.475	1.497	1.441
11	1.593	1.518	1.747	1.629	1.583	1.564	1.606
12	1.489	1.416	1.335	1.448	1.471	1.466	1.438
13	1.931	1.968	1.918	1.948	1.968	2.034	1.961
14	2.085	2.088	1.985	2.054	2.046	1.987	2.041
15	2.054	2.052	2.018	2.060	2.079	1.991	2.042
16	1.899	1.975	2.066	1.852	2.044	1.986	1.970
17	2.195	2.216	2.215	2.158	2.178	2.251	2.202
18	2.118	2.081	2.135	2.156	2.201	2.121	2.135
19	2.809	2.842	2.836	2.849	2.775	2.759	2.812
20	2.845	2.932	2.928	2.991	2.904	2.889	2.915
21	2.880	2.786	2.886	2.738	2.827	2.867	2.831
22	2.754	2.785	2.721	2.852	2.734	2.778	2.771
23	2.795	2.789	2.752	2.787	2.694	2.702	2.753
24	2.702	2.704	2.624	2.672	2.711	2.672	2.681
25	3.363	3.309	3.368	3.379	3.360	3.299	3.346
26	3.173	3.208	3.283	3.276	3.274	3.129	3.224
27	3.353	3.499	3.450	3.391	3.566	3.328	3.431
28	3.377	3.387	3.390	3.362	3.407	3.467	3.398
29	3.319	3.221	3.313	3.360	3.153	3.209	3.263
30	3.417	3.387	3.503	3.484	3.627	3.645	3.511

3.3. Acquisition of milling workpiece images and making of the data set

3.3.1. Acquisition of milling workpiece images

The milling workpiece image capturing device is shown in Fig. 7a, consisting of a Basler color CCD camera equipped with a VS-2514H1industrial lens, two OPT-LI14030white strip light sources, an OPT-DPA1024E-4 digital current controller, a TES-1332A digital illuminance meter and an experimental stand. To obtain more details of the milling surface roughness, the milling workpiece was placed flat on the measurement platform, the camera optical axis was perpendicular to the measured surface, and the white strip light source was fixed on the experimental stand at a suitable angle. The relative positions of the CCD camera and light source were maintained

www.czasopisma.pan.pl   PAN   www.journals.pan.pl
POLSKA AKADEMIA NAUK

R. Fang et al.: CLASSIFICATION AND INSPECTION OF MILLING SURFACE ROUGHNESS BASED ON A BROAD LEARNING ...

throughout the experiment, the ambient luminance was adjusted using a digital current controller, and the ambient illuminance was measured using the illuminance meter with a value of 757 LUX.
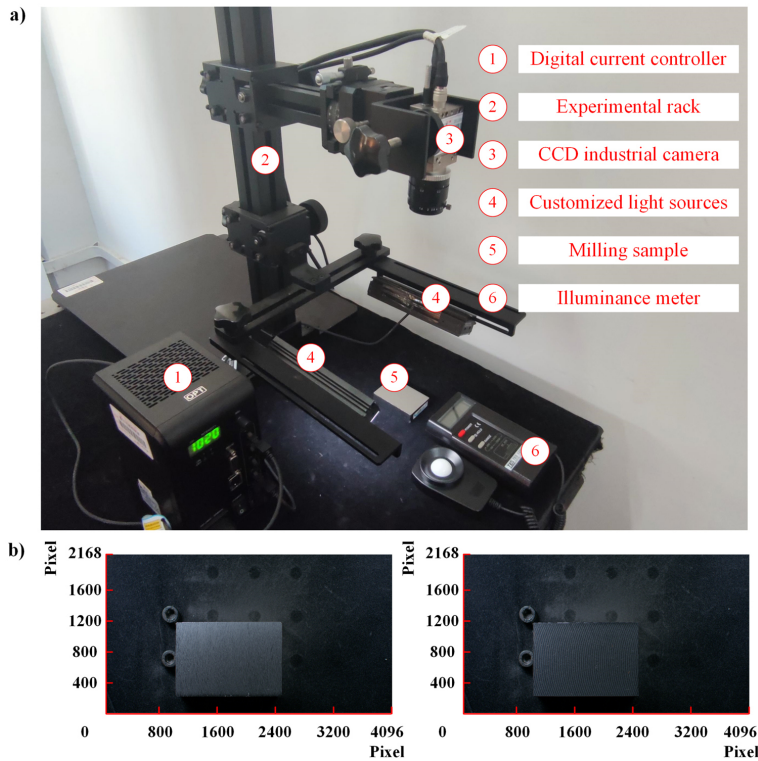
Fig. 7. a) Diagram of the experimental setup, b) milling workpiece image.

In addition, to increase the diversity of the data, the position of the workpiece was adjusted appropriately as needed during the shooting process. Fig. 7b shows a portion of the acquired images, each with a size of 4096 × 2168 pixels. As can be seen in Fig. 7b, the image quality of the workpiece was not only affected by the lighting conditions but also related to the surface morphology of the workpiece, showing the uneven distribution of light and dark and reflective phenomena. These factors make the construction of the roughness measurement model harder.

3.3.2. Dataset making

The 30 milling workpieces in Table 2 were divided into 5 roughness grades, with 6 workpieces in each grade. 4 workpieces in each grade were taken as training workpieces and the remaining 2 workpieces were testing workpieces. In addition, in the same milling workpiece image, although the workpiece surface is all of the same roughness value, there are subtle differences in various parts of the surface, so the image can be cut into several pieces for separate processing. This approach can increase the number of workpiece images to improve the performance of the model. Therefore, the area where the milling workpiece was located in each original image divided into six areas of 450 × 466 pixels in size without overlapping each other (Fig. 8). Then the original images were cropped according to the divided area to obtain a train set containing 720 images of

milling workpieces and a test set containing 360 images of milling workpieces. This means that in the original dataset, the ratio of the train set to the test set is 4:2.
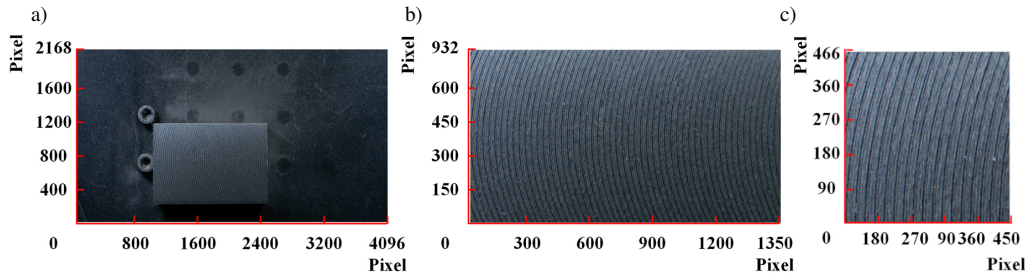
Fig. 8. (a) The original. (b) The area where the milling workpiece is located. (c) The final cut.

One test milling workpiece image was selected from the test set according to each of the five roughness levels (Fig. 9). From Fig. 9, it can be found that the milling surface topography had more obvious changes as the roughness increased, especially the texture features, consistent with the analysis of the milling surface morphology in Section 2.1, improving the feasibility of the experiment.
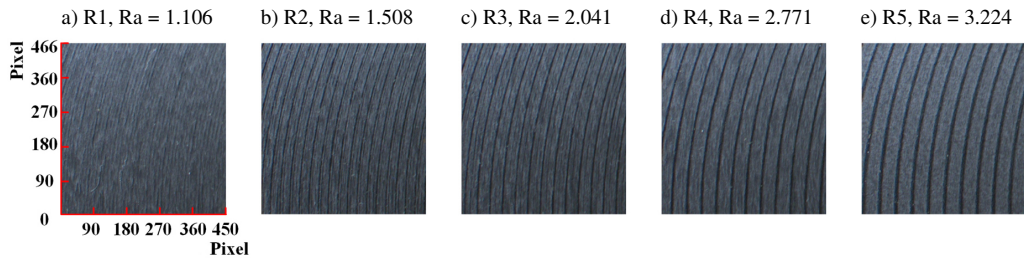
Fig. 9. Milling sample images for each roughness grade.

Finally, the milling workpiece images in the train set were data-enhanced according to the method described in Section 2.3, and the sample classification and number statistics after data enhancement are shown in Table 3. It should be noted that the milling workpiece images in the test set were not data-enhanced to be closer to the actual inspection environment of milling workpieces.

Table 3. Sample classification and number statistics before and after data enhancement.

Roughness (µm)		R1 [1–1.4]	R2 [1.4–1.9]	R3 [1.9–2.5]	R4 [2.5–3.1]	R5 [3.1–3.7]	Total
Train set	Before data enhancement	144	144	144	144	144	720
	After data enhancement	1440	1440	1440	1440	1440	7200
Test set		72	72	72	72	72	360

www.czasopisma.pan.pl   **PAN**   www.journals.pan.pl
POLSKA AKADEMIA NAUK

R. Fang et al.: CLASSIFICATION AND INSPECTION OF MILLING SURFACE ROUGHNESS BASED ON A BROAD LEARNING...

3.4. Comparison experiments

3.4.1. BLS model

Similar to the deep learning model, the parameter search of the BLS model also includes internal and external optimizations. During the training process, internal optimization refers to adjusting the weights of each layer of the network. The external optimization search mainly includes the number of feature nodes $N1$ within each window of the mapping layer, number of mapping layer windows $N2$, number of enhancement nodes $N3$, regularization parameter λ and shrinkage parameter S. Among others, in the literature, [18], we find that the classification performance of the BLS depended greatly on $N1$, $N2$ and $N3$. Therefore, in order to construct a roughness measurement model with better performance, an orthogonal experiment [19] was used to analyze the effects of $N1$, $N2$, and $N3$ on the model performance. The experimental results are shown in Fig. 10.
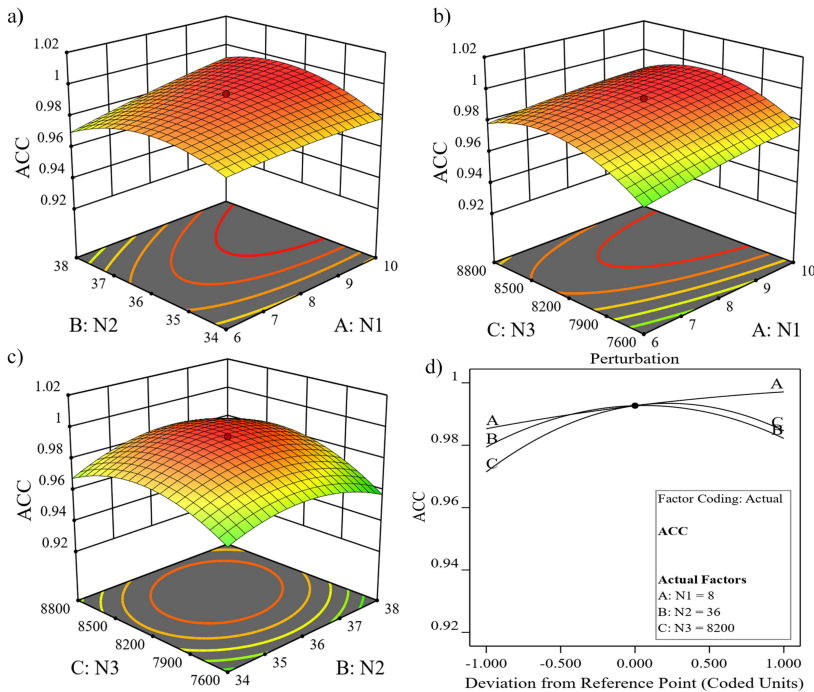
Fig. 10. 3D response surface diagram and perturbation diagram, ACC (accuracy).

From Figs. 10a and 10b, it can be seen that the change in accuracy was smaller when $N1$ was changed. When $N2$ and $N3$ were gradually increased, the accuracy showed a trend of increasing and then decreasing. This demonstrated that increasing the number of feature nodes and enhancement nodes appropriately could significantly strengthen the sample features. It improved the ability to discern between distinct categories. However, an excess of feature nodes and augmentation nodes would bring attributes that partially overlap with the initial semantic attribute space, resulting in generation of redundant information. This redundancy had significant interference with the classifier, which eventually led to the degradation of classification accuracy.

As shown in Fig. 10c, there were circular intervals in the contour plot, which indicated that the highest accuracy existed in the interval {$N2$ [35, 37], $N3$ [7900, 8500]}. In addition, it can also be seen from Fig. 10d that the curves bend from large to small as $C > B > A$, which indicated that the degree of influence of each parameter on the accuracy was ranked from large to small as $N3 > N2 > N1$.

It is worth noting that the BLS enables dynamic updating of the system, updating the weights of the system instantly for newly added nodes, which greatly reduces the time of parameter search [16]. The model is simple, fast and easy to update compared to classical deep learning models. In combination with the orthogonal experimental analysis, the external parameters of the model were determined through a series of pre-experiments (Table 4) where $N1 = 8$, $N2 = 36$, $N3 = 8200$, $\lambda = 2^{-30}$, $S = 0.8$. Finally, the data set of Table 3 was fed into the BLS model for training.

Table 4. Parameter setting of the BLS.

λ	S	$N1$	$N2$	$N3$
2^{-30}	0.8	8	36	8200

3.4.2. Comparison model

To better evaluate the prediction performance of the BLS model, the following comparison experiments designed are presented in this paper.

1. The basic idea of a *support vector machine* (SVM) is to map data to a high-dimensional feature space through a nonlinear mapping and then perform feature classification in this high-dimensional space [20]. In the literature, [6], the surface topography images of a deep hole were analyzed with the *gray-level co-occurrence matrix* (GLCM) method, and several features of image, which were nearly monotonic with the surface roughness, were extracted to fabricate a prediction model of the roughness of the deep-hole surface accurately. Moreover, the SVM model was presented to describe the relationship of GLCM features and the actual surface roughness. In the literature, [7], the five spectrum index measures of surface roughness were extracted in the spatial frequency domain using a two-dimensional Fourier transform. Two artificial neural networks which took roughness features as the input were developed to determine the surface roughness. Based on the study above, an SVM model based on five spectrum indices (FR-SVM) was proposed as the comparison model. The model parameters are shown in Table 5.

Table 5. Parameter Setting of FR-SVM.

Coding	Learner weights	Kernel function	Prior
One-vs-one	0.4	linear	0.2

2. The Residual Network (Resnet) proposed by He *et al.* [21] has an important position in the field of deep learning. It can build a deeper network layer by introducing the residual network structure and the final classification results are excellent. Many subsequent methods were built on the basis of Resnet50 or Resnet101. To better evaluate the advantages and disadvantages of broad learning and deep learning, Resnet50v2 [22], a classical image classification algorithm for deep learning, was selected as the comparison model in this paper. The model parameters are shown in Table 6. Both of the two comparison models above were subjected to a series of pre-experiments.

www.czasopisma.pan.pl PAN www.journals.pan.pl
POLSKA AKADEMIA NAUK

R. Fang et al.: CLASSIFICATION AND INSPECTION OF MILLING SURFACE ROUGHNESS BASED ON A BROAD LEARNING . . .

Table 6. Parameter Setting of Resnet50v2.

Batch	Epoch	Optimizers	Learning rate
32	100	Adam	0.0001

3.4.3. Model evaluation standards

Three common evaluation standards were selected to validate the model performance of the model, including confusion matrix, accuracy, ROC curve and AUC value [23, 24]. The model performance of each evaluation standard response is shown in Table 7.

Table 7. Evaluation standards.

Confusion Matrix	The confusion matrix represents a standard format for accuracy evaluation and is used to observe the performance of the model on each category.
Accuracy	The accuracy indicates the proportion of all samples correctly predicted.
ROC curves and AUC values	The ROC curve responds to the generalization ability of the model, and the AUC responds to the classification model's ability to rank the samples.

3.5. Analysis and discussion of experimental results

3.5.1. Experimental results

To reasonably evaluate the ability of the model to measure the surface roughness of milling workpieces, the experiments were conducted using the test set in Table 3 for the trained FR-SVM, Resnet50v2 and BLS, and the results are shown in Table 8.

Table 8. Experimental results of each model.

Model	Accuracy (%)	Training Time
FR-SVM	55.6	89s
Resnet50v2	99.2	34m57s
BLS	99.4	169s
	BLS ≈ Resnet50v2 > FR-SVM	Resnet50v2 > BLS > FR-SVM

From Table 8, it can be seen that: (1) The classification effect of FR-SVM was much lower than that of Resnet50v2 and BLS, with an accuracy of only 55.6%. In creating the indices, the strategy may have lost a lot of image information, resulting in the model's low classification performance. In addition, while FR-SVM required less time to train than the other two models (89s), the process of designing indices was time-consuming and computationally challenging, thus limiting the method's usefulness. (2) Secondly, although Resnet50v2 had a high accuracy rate of 99.2% and was able to extract automatically, the model training was extremely time-consuming. The whole training process took a total of 34 minutes and 57 seconds (34m57s), 12.4 times longer than that of BLS. (3) Compared with the previous two models, the BLS exhibited excellent performance in milling surface roughness classification detection with fast and high accuracy: the accuracy was as high as 99.4%, 43.8% higher than FR-SVM and similar to Resnet50v2; the model training time was 169s, only 8% of Resnet50v2. The result proved that the BLS model not only can extract features by itself, but also has excellent performance in terms of accuracy and training time.

3.5.2. Model performance evaluation

1. To visualize the recognition ability of BLS, FR-SVM and Resnet50v2 at each roughness grade, the prediction results were visualized by a confusion matrix, as shown in Fig. 11. Each value on the main diagonal represents the number of correctly classified samples, and a darker color indicates a larger number.
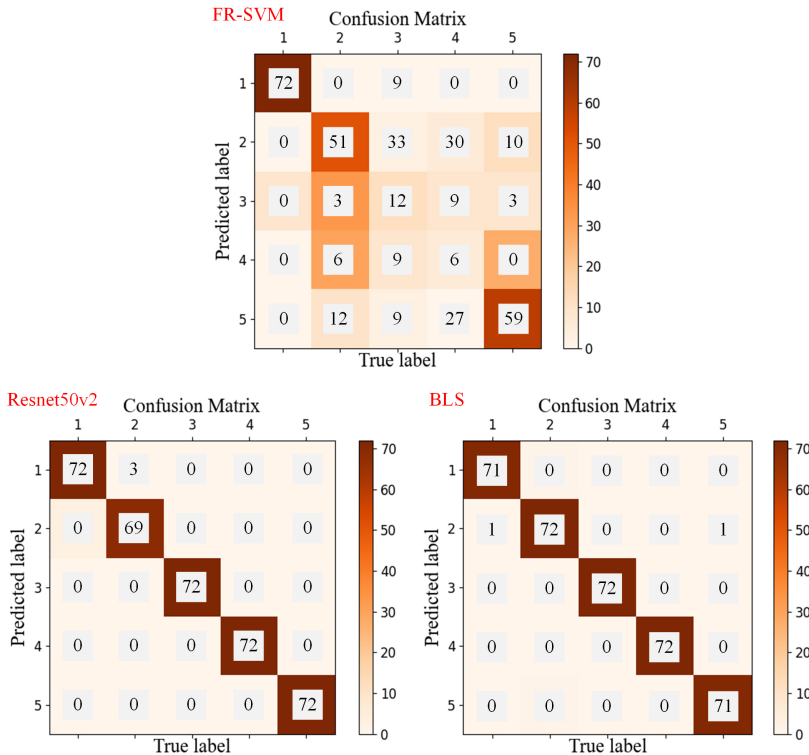
Fig. 11. Confusion matrix for each model.

From Fig. 11, it was found that FR-SVM achieved higher classification accuracy for R1, and the rest of the categories were much lower than R1. When predicted using Resnet50v2, the best classification results were achieved for R3, R4, and R5, and the other two categories showed little difference from the best results. Similarly, BLS realized the best classification results for R3 and R4 and achieved suboptimal classification in the other categories. The analysis above showed that the accuracy of both BLS and Resnet50v2 reached a high level without a great difference, while the difference was larger between FR-SVM and the first two.

2. Since the analysis results above only reflect the classification accuracy of each model, the ROC curve and AUC were utilized to evaluate the generalization ability of the model and the ranking ability of the samples. The results are shown in Fig. 12.

From Fig. 12, it is observed that all the ROC curves of Resnet50v2 were close to the upper left corner of the figure with an average AUC of 1. It was shown that Resnet50v2 had an excellent generalization ability and a strong ranking ability for milling samples. Although BLS's ROC1 and ROC2 curves strayed somewhat from the upper left corner, the ROC curves and AUCs for the remaining three categories were comparable to those of Resnet50v2, with the average AUC
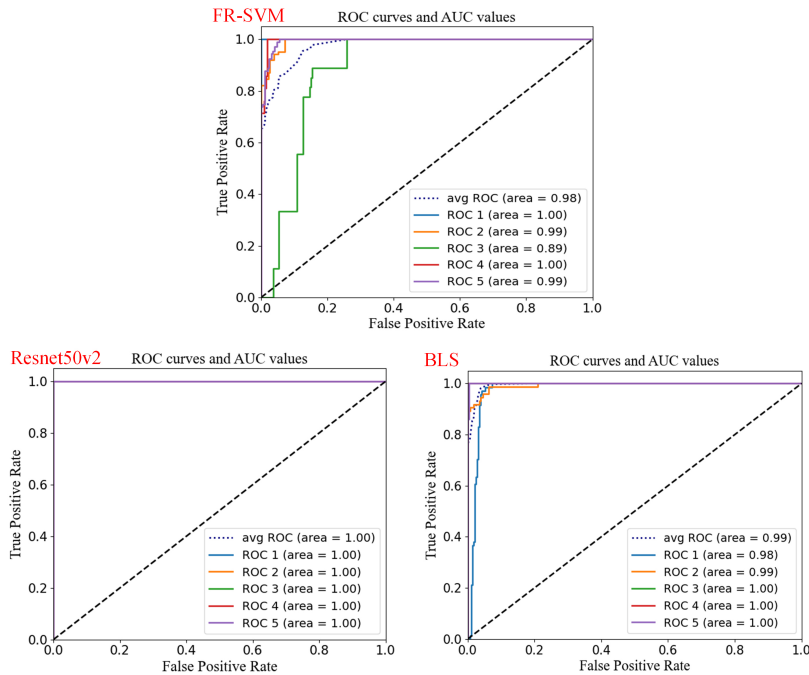
Fig. 12. ROC curves and AUC values for each model.

reaching 0.99. It indicated that BLS also had satisfactory generalization ability and sample sorting ability. Compared with the first two, FR-SVM had the weakest generalization ability and sample sorting ability, especially the ROC3 curve had a more obvious deviation. Therefore, Resnet50v2 exhibited the best generalization ability and sample sorting ability, followed by BLS and, finally, FR-SVM.

The BLS, Resnet50v2 and FR-SVM are summarized in terms of prediction accuracy, model training speed, generalization ability and sample sorting ability.

1. In terms of prediction accuracy, BLS and Resnet50v2 were close to each other, both reaching 99%. At the same time, FR-SVM was far inferior to them, with only 55.6%.
2. In terms of training speed, FR-SVM greatly outperformed BLS and Resnet50v2. The training time of FR-SVM was only 89 s, while that of BLS and Resnet50v2 was 169 s and 34 m 57 s, respectively.
3. In terms of generalization ability and sample sorting ability, Resnet50v2 performed the best, followed by BLS, and FR-SVM performed the worst. Table 9 shows the performance comparison of each model.

Table 9. Performance comparison of each model.

Accuracy	Training Speed
BLS ≈ Resnet50v2 > FR-SVM	FR-SVM > BLS > Resnet50v2
Generalization ability	**Sample sorting ability**
Resnet50v2 > BLS > FR-SVM	Resnet50v2 > BLS > FR-SVM

3.5.3. Discussion of different machine learning methods

As shown in Fig. 13, different machine learning methods were analyzed in terms of feature processing, data dependency, model training speed, and generalization ability based on the roughness measurement task.
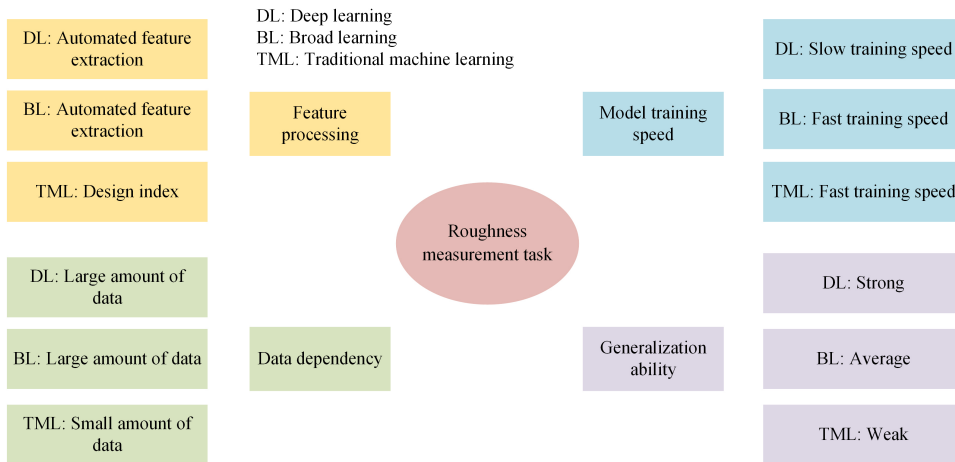
Fig. 13. Different machine learning methods and their characteristics.

A summary information for the machine methods analyzed is presented below:

1. Feature processing. In most of the traditional machine learning based roughness measurement methods, image features need to be designed as indices, and the features can be pixel values, shapes, textures, *etc*. The performance of this approach is contingent upon the accuracy of the retrieved features. By contrast, deep and broad learning attempt to extract high-level information directly from the image of the milling workpiece. On this basis, deep learning and broad learning significantly reduce the effort required to construct feature extractors for roughness measurement problems.

2. Data dependency. The performance of deep learning and broad learning depends on a large amount of data. For example, the desirable roughness prediction model cannot be trained with too few milling data because both types of models require a large amount of data to learn to recognize milling workpieces. On the other hand, traditional machine learning algorithms using human-designed indices may perform better when the amount of data is small.

3. Model training speed. Deep learning algorithms have many parameters, so it takes a long time to train the algorithm. In comparison, the broad learning's network structure is fairly simple due to the absence of multiple layers of connections, and training speed is significantly increased. Additionally, classical machine learning has a faster training speed due to the feature engineering stage.

4. Generalization ability. The deep learning network can extract more abstract features from the milling training data, which makes its generalization ability extremely good. Broad learning can learn important features from the milling training data and achieve a high fit to the data. However, the features learned by the broad learning network are simpler, which makes it not as good at generalization as the deep learning network. Compared to them, traditional machine learning methods use feature indices that are designed by the researcher for a particular scenario. When the conditions change, the prediction becomes worse, resulting in the worst generalization performance.

4. Conclusions

The existing index design-based and deep learning-based roughness measurement methods experience problems such as difficult index design, large human influence factors and slow model training speed. In this paper, based on the broad learning system and combined with image data enhancement algorithms, a visual measurement method for surface roughness of milling workpieces was proposed based on the broad learning system. The method could significantly accelerate the model training speed and automatically extract the image features related to the roughness of the milling workpiece surface. For the milling workpiece roughness measurement, its recognition accuracy achieved 99.4%, and the training time was only 169s. In comparison with other roughness measurement models, the BLS model was able to maintain a high recognition accuracy with a very short training time. It proved that the model proposed in this paper has the potential to be a fast real-time roughness measurement system, and provided a technical support for the rapid inspection of online vision under common light source in industrial production.

In the future, we will consider the effects of different lighting conditions as well as shooting angles on the model performance based on this method. This helps to improve the robustness of the model to lighting changes and shooting angle changes, and increases the feasibility of deploying the model in real variable lighting environments.

Acknowledgements

Appendix I. Nomenclature

Abbreviations	Definition
BLS	Broad learning system
Resnet	Residual Network
SVM	support vector machine
GLCM	gray-level co-occurrence matrix
RVFLNN	random vector functional-link neural network
ROC	Receiver Operating Characteristic curve
AUC	Area under the Curve

Symbol	Definition
X	input data
A	input layer
Y	output layer
Z_i	feature node
Z^n	feature node group
H_j	enhancement node
H^m	enhancement node group
W	connection weight between the input layer A and the output layer Y
W_{fi}	random weight matrix
ϕ_i	mapping function
b_{fi}	random bias matrix
$N1$	number of feature nodes within each window of the mapping layer

$N2$	number of mapping layer windows
$N3$	number of enhancement nodes
λ	number of enhancement nodes
S	shrinkage parameter
Ra	roughness parameters

Parameter Name	Setting
$N1$	8
$N2$	36
$N3$	8200
λ	2^{-30}
S	0.8
Coding	One-vs-one
Learner Weights	0.4
Kernel Function	linear
Prior	0.2
Batch	32
Epoch	100
Optimizers	Adam
Learning rate	0.0001

References

[1] He, B., Ding, S., & Shi, Z. (2021). A comparison between profile and areal surface roughness parameters. *Metrology and Measurement Systems*, *28*(3), 413–438. https://doi.org/10.24425/mms.2021.137133

[2] He, B., Zheng, H., Ding, S., Yang, R., & Shi, Z. (2021). A review of digital filtering in evaluation of surface roughness. *Metrology and Measurement Systems*, *28*(2). https://doi.org/10.24425/mms.2021.136606

[3] Mathia, T. G., Pawlus, P., & Wieczorowski, M. (2011). Recent trends in surface metrology. *Wear*, *271*(3-4), 494–508. https://doi.org/10.1016/j.wear.2010.06.001

[4] Yilbas, Z., & Hasmi, M. S. J. (1999). Surface roughness measurement using an optical system. *Journal of Materials Processing Technology*, *88*(1–3), 10–22. https://doi.org/10.1016/S0924-0136(98)00356-2

[5] Chang, H. K., Kim, J. H., Kim, I. H., Jang, D. Y., & Han, D. C. (2007). In-process surface roughness prediction using displacement signals from spindle motion. *International Journal of Machine Tools and Manufacture*, *47*(6), 1021–1026. https://doi.org/10.1016/j.ijmachtools.2006.07.004

[6] Liu, W., Tu, X., Jia, Z., Wang, W., Ma, X., & Bi, X. (2013). An improved surface roughness measurement method for micro-heterogeneous texture in deep hole based on gray-level co-occurrence matrix and support vector machine. *The International Journal of Advanced Manufacturing Technology*, *69*(1), 583–593. https://doi.org/10.1007/s00170-013-5048-0

[7] Tsai, D. M., Chen, J. J., & Chen, J. F. (1998). A vision system for surface roughness assessment using neural networks. *The International Journal of Advanced Manufacturing Technology*, *14*(6), 412–422. https://doi.org/10.1007/BF01304620

[8] Huaian, Y. I., Jian, L. I. U., Enhui, L. U., & Peng, A. O. (2016). Measuring grinding surface roughness based on the sharpness evaluation of colour images. *Measurement Science and Technology*, *27*(2), 025404. https://doi.org/10.1088/0957-0233/27/2/025404

[9] Yi, H., Liu, J., Ao, P., Lu, E., & Zhang, H. (2016). Visual method for measuring the roughness of a grinding piece based on color indices. Optics express, 24(15), 17215–17233. https://doi.org/10.1364/OE.24.017215

[10] Huaian, Y., Xinjia, Z., Le, T., Yonglun, C., & Jie, Y. (2020). Measuring grinding surface roughness based on singular value entropy of quaternion. *Measurement Science and Technology*, *31*(11), 115006. https://doi.org/10.1088/1361-6501/ab9aa9

[11] Chen, Y., Yi, H., Liao, C., Huang, P., & Chen, Q. (2021). Visual measurement of milling surface roughness based on Xception model with convolutional neural network. *Measurement*, *186*, 110217. https://doi.org/10.1016/j.measurement.2021.110217

[12] Rifai, A. P., Aoyama, H., Tho, N. H., Dawal, S. Z. M., & Masruroh, N. A. (2020). Evaluation of turned and milled surfaces roughness using convolutional neural network. *Measurement*, *161*, 107860. https://doi.org/10.1016/j.measurement.2020.107860

[13] He, Y., Zhang, W., Li, Y. F., Wang, Y. L., Wang, Y., & Wang, S. L. (2021). An approach for surface roughness measurement of helical gears based on image segmentation of region of interest. *Measurement*, *183*, 109905. https://doi.org/10.1016/j.measurement.2021.109905

[14] Pao, Y. H., Park, G. H., & Sobajic, D. J. (1994). Learning and generalization characteristics of the random vector functional-link net. *Neurocomputing*, *6*(2), 163–180. https://doi.org/10.1016/0925-2312(94)90053-1

[15] Twardowski, P., Wojciechowski, S., Wieczorowski, M., & Mathia, T. (2011). Surface roughness analysis of hardened steel after high-speed milling. *Scanning*, *33*(5), 386–395. https://doi.org/10.1002/sca.20274

[16] Chen, C. P., & Liu, Z. (2017). Broad learning system: An effective and efficient incremental learning system without the need for deep architecture. *IEEE Transactions on Neural Networks and Learning Systems*, *29*(1), 10–24. https://doi.org/10.1109/TNNLS.2017.2716952

[17] McDonald, G. C. (2010). Tracing ridge regression coefficients. *Wiley Interdisciplinary Reviews*: *Computational Statistics*, *2*(6), 695–703. https://doi.org/10.1002/wics.126

[18] Lei, M., Rao, Z., Li, M., Yu, X., & Zou, L. (2019). Identification of coal geographical origin using near infrared sensor based on broad learning. *Applied Sciences*, *9*(6), 1111. https://doi.org/10.3390/app9061111

[19] Jiaqiang, E., Han, D., Qiu, A., Zhu, H., Deng, Y., Chen, J., Zhao, X., Zuo, W., Wang, H., Chen, J., & Peng, Q. (2018). Orthogonal experimental design of liquid-cooling structure on the cooling effect of a liquid-cooled battery thermal management system. *Applied Thermal Engineering*, *132*, 508–520. https://doi.org/10.1016/j.applthermaleng.2017.12.115

[20] Aburomman, A. A., & Reaz, M. B. I. (2017). A novel weighted support vector machines multiclass classifier based on differential evolution for intrusion detection systems. *Information Sciences*, *414*, 225–246. https://doi.org/10.1016/j.ins.2017.06.007

[21] He, K., Zhang, X., Ren, S., & Sun, J. (2016). Deep residual learning for image recognition. In Proceedings of the IEEE Conference on Computer Vision and Pattern Recognition (pp. 770–778). https://doi.org/10.1109/CVPR.2016.90

[22] Karar, M. E., Hemdan, E. E. D., & Shouman, M. A. (2021). Cascaded deep learning classifiers for computer-aided diagnosis of COVID-19 and pneumonia diseases in X-ray scans. *Complex & Intelligent Systems*, *7*(1), 235–247. https://doi.org/10.1007/s40747-020-00199-4

[23] Zeng, G. (2020). On the confusion matrix in credit scoring and its analytical properties. *Communications in Statistics – Theory and Methods*, *49*(9), 2080–2093. https://doi.org/10.1080/03610926.2019.1568485

[24] Carrington, A. M., Fieguth, P. W., Qazi, H., Holzinger, A., Chen, H. H., Mayr, F., & Manuel, D. G. (2020). A new concordant partial AUC and partial c statistic for imbalanced data in the evaluation of machine learning algorithms. *BMC Medical Informatics And Decision Making*, *20*(1), 1–12. https://doi.org/10.1186/s12911-019-1014-6

Runji Fang received his B.S. degree from Guilin University of Technology in 2020. At present, he is a current graduate student of Guilin University of Technology. His main research interest is machine vision.

Huaian Yi received his B.S. degree from Xiangtan University in 1997, his M.S. degree from Kunming University of Science and Technology in 2008, and his Ph.D. degree from Hunan University in 2017. At present, he is an associate professor at Guilin University of Technology. His main research interest is machine vision.

Shuai Wang is an undergraduate student at Guilin University of Technology. His main research interest is machine vision.

Yilun Niu is a undergraduate student at Guilin University of Technology. His main research interest is machine vision.